1 **Continuous fixed-bed column studies to remove polycyclic aromatic hydrocarbons by**
2 **degrading enzymes immobilized on polyimide aerogels**
3
4 **Seyyed Mohammadreza Davoodi[1], Saba Miri[1], Satinder Kaur Brar[1*], Richard Martel[3]**

5

6

7 [1] Department of Civil Engineering, Lassonde School of Engineering, York University, North York,
8 Toronto, Ontario Canada M3J 1P3.
9
10 [2] INRS-ETE, Université du Québec, 490, Rue de la Couronne, Québec, Canada G1K 9A9

11
12 (*Phone: 1 418 736 2100 ext. 55228; E-mail: Satinder. brar@lassonde.yorku.ca)
13

14

Abstract:

16

17 The main sources of polycyclic aromatic hydrocarbons, entering aquatic environments are
18 industrial discharges, petroleum spills, combustion of fossil fuels, urban runoff, and atmospheric
19 deposition. For the biodegradation of polycyclic aromatic hydrocarbons, the use of biocatalysts,
20 such as enzymes, is an environmentally friendly method. Despite this, it is necessary to immobilize
21 the enzymes in order to facilitate their recovery and reusability, as well as to prevent their loss.
22 Using covalent bonding, PAH degrading enzymes were immobilized on modified polyimide
23 aerogels. Covalent immobilization of enzymes on modified polyimide aerogels resulted in around
24 9- and 6-fold lower enzyme leaching for naphthalene and catechol 2,3 dioxygenase enzymes
25 compared to enzyme immobilization using adsorption. The Fourier Transform Infrared Spectrum
26 (FTIR) confirmed the enzyme immobilization and aerogel modification. The effects of flow rate,
27 size of aerogels and inlet concentration of anthracene on removal efficiency of pollutant were
28 examined. Using the derived model as a basis for prediction, In terms of removal efficiency, the
29 highest result was achieved to be 84.01% at flow rate of 22 ml min^{-1}, initial concentration of 34
30 mg l^{-1} and aerogel size 2 cm while under these conditions, the removal efficiency was
31 experimentally measured to be 87.14 %. Enzyme loaded-aerogel as a fixed-bed column for the
32 removal of polycyclic aromatic hydrocarbons provides novel insight into the application of aerogel
33 base materials for water treatment and PAH removal with possibilities of scaling up for larger
34 applications.

35

36

37 **Keywords**: polycyclic aromatic hydrocarbons; Enzymatic bioremediation; Fixed-bed columns

38

1. Introduction:

There is a frequent threat of environmental contamination, including contamination of water bodies and soils by oil spills. This is particularly relevant for both the United States and Canada where the transportation of unconventional oils and traditional petroleum over long distances inland is accomplished by railways and pipelines. Moreover, during oil exploration, wastewater is generated that contains dissolved and dispersed oil, grease, salts, heavy metals, and other organic and inorganic substances (Zabbey and Olsson, 2017). Many aromatic hydrocarbons, polycyclic aromatic hydrocarbons, and heterocyclic compounds are present in petroleum products. Researchers have traditionally assessed the toxic effects of oil by measuring the concentration of polycyclic aromatic hydrocarbons (PAHs) since PAHs are often regarded as the most toxic fraction of oil. As a result, many water samples collected from the field during and after the oil spill were analyzed for these compounds (Davoodi et al., 2020).

Biocatalysts such as enzymes have an important role to play in industrial processes, biosensors, and biofuel cells (Çakmakçı et al., 2014). Good enzyme stability is a key requirement for these applications. The in vitro development of enzymatic cascade reactions has been inspired by biodegradation processes, in which multiple enzymes work together. The multi- enzyme immobilization could enhance the overall efficiency and specificity of the reaction, omitting the need to isolate intermediate products. The multi- enzyme immobilization recently been demonstrated on a few substrates such as magnetic particles. Our rationale is that ideal immobilization materials should be cost-effective, trap enzymes under mild conditions, allow easy substrate access, prevent enzyme leaching, and provide enzyme protection. Unfortunately, most of the above materials do not meet all these criteria (Kadri et al., 2018a). Most recently, Miri *et.al* studied the effectiveness of co-immobilization of cold-active enzymes involved in biodegradation of monoaromatic hydrocarbons on micro/nano biochar particles. They showed that immobilization of toluene dioxygenase and catechol 2,3 dioxygenase enhanced their storage and operational stability.(Miri et al., 2021b)

Generally, it is necessary to develop an efficient method of immobilizing enzymes to facilitate their recovery and reusability while avoiding their loss (Simón-Herrero et al., 2019). Enzymes can be immobilized by several methods, including covalent, adsorption, crosslinking, encapsulation, and entrapment (Rodríguez-Delgado and Ornelas-Soto, 2017). Most commonly, covalent attachment is used to prevent enzyme leaching and improve enzyme stability. Compared to other methods of immobilization, it is more stable within the reaction system and provides strong attachment. To maintain high catalytic activity, it is important that the structure of enzyme is protected from the severe reaction conditions (Zucca and Sanjust, 2014). In addition, stable enzyme-matrix interactions are necessary as well as effective enzyme-matrix binding by increasing the affinity between the functional groups on the support and the enzymes (Zdarta et al., 2018b). Simón-Herrero *et.al* proposed the laccase-loaded polyimide aerogels for carbamazepine biodegradation to facilitate enzyme recovery and reusability. (Simón-Herrero et al., 2019)

In order to achieve effective enzyme immobilization, support materials must be chemically and thermally stable, high affinity to biomolecules, insoluble in reaction conditions, biocompatible,

81 contain reactive functional groups, regenerating and reusable, and readily available and affordable
82 (Zdarta et al., 2018a). As inorganic supports are known to have several limitations, such as low
83 affinity to enzymes, limited biocompatibility, and the limited possibility to create various organic
84 materials and geometrical shapes such as synthetic polymers have increasingly been used as
85 supports. Moreover, synthetic polymers have some advantages such as being tailored to meet the
86 needs of specific enzymes and processes, they have some advantages. Many functional groups are
87 present in these materials, such as trialkyl amines and hydrophobic alkyl groups, as well as epoxy,
88 carboxyl, carbonyl hydroxyl, amine, and diol groups, facilitating enzyme binding and surface
89 functionalization (Zdarta et al., 2018b). Nanoparticles can also be used to encapsulate enzymes.
90 For example, Kadri et.al reported the entrapment of crude alkane hydroxylase and lipase enzymes
91 into chitosan nanoparticles by the ionotropic gelatin method. However, nanoparticles may not be
92 suitable for enzyme encapsulation due to their less porous structure, enzymes may have difficulty
93 accessing substrates. However, polyimide aerogels has excellent thermal and mechanical
94 properties, polyimide may be suitable support material for enzyme immobilization (Murphy,
95 2016). Considering the benefits of polyimide aerogels as support materials for enzyme
96 immobilization, they may be a promising alternative. Furthermore, the polyimide aerogels can be
97 produced using an environmentally friendly freeze-drying process.
98 In this study, covalent immobilization of PAH degrading enzymes on modified polyimide aerogels
99 was studied and the application of prepared immobilized enzymes in a fixed bed column was
100 examined. The effect of inlet concentration and flowrate parameters upon the removal of target
101 pollutants was discussed to acheive an estimation of optimum values of the operational variables
102 for efficient removal of pollutants through the fixed bed column.
103
2. Materials and Methods

2.1. Chemicals

106 This study used Poly (pyromellitic dianhydride-co-4,4′-oxydianiline) amic acid solution from
107 Sigma-Aldrich in order to conduct the experiment. Glutaraldehyde (25%), methanol, and
108 ethylenediamine were purchased from Sigma-Aldrich. The following
109 analytical/microbiological grade chemicals were all purchased from Fisher Scientific (Ontario,
110 Canada) for enzyme preparation: dichloromethane, tryptic soy broth/agar (TSB, TSA), KNO_3,
111 NaCl, Ca_2CO_3, Na_2HPO_4, KH_2PO_4, NaOH, and HCl, yeast extract. Nutrient broth (NB) medium
112 was purchased from Sigma-Aldrich Co. (USA). The strains used for enzyme production are newly
113 isolated *Pseudomonas* URS-5, URS-6, URS-8 and *Rhodocucus* URS-10 (Davoodi et al.).

2.2. Production of the enzymes

115 PAH degrading enzymes were produced via multi-culture of psychrophilic *Pseudomonas*,
116 *Rhodococcus* strains as reported in previous work (Davoodi et al.). In brief, 50 ppm of
117 anthracene solution in methanol was mixed with autoclaved at $120 \pm 1\ ℃$ nutrition broth
118 in 50 ml Erlenmeyer flasks. After that, the inducers were inoculated with consortia
119 including URS-6,8,10 incubated at $15 \pm 1\ ℃$ for 2 days. For enzyme extraction, cells were
120 harvested from the media after culturing by centrifugation (16,000 rpm for 4 min at 4 °C). The
121 pellets with the biomass were resuspended in phosphate buffer, pH 6.5, and then sonicated on ice

122 using an Ultrasonicator (Branson Ultrasonics Corporation, Danbury, CT, USA) at 22 and 30 kHz

123 frequencies of ultrasounds for 10 min to obtain intracellular enzymes.

2.3. Preparation of polyimide aerogels

125 A solution of triethylamine (TEA) was first prepared in deionized water, before being stirred in an

126 ultrasound bath. The TEA-water solution was then added with 3 wt % dried poly (amic acid) PAA,

127 and the solution was stirred for a few minutes. Using the laboratory freeze-dryer, trays were filled

128 with PAA/TEA-water solution, and they were then frozen at 60 °C and then sublimed under a

129 vacuum to obtain PAA aerogel. Polyimide aerogel was obtained by thermal imidizing PAA aerogel

130 in a vacuum oven. The color has changed from white to bright yellow. The Fourier Transform

131 Infrared Spectrum (FTIR) was used to confirm the thermal imidization.

2.4. Polyimide aerogel surface modification

133 In accordance with previous studies on polyimide aerogels, modifications were made to

134 them (Simón-Herrero et al., 2019). Polyimide aerogels (1 g) were aminated by immersing in a

135 10% w/v solution of ethylenediamine in methanol for 1 hour. In order to remove residual

136 ethylenediamine, the modified aerogel was immediately washed with methanol. In order to

137 completely remove methanol from the modified aerogel, it was removed from the oven after 24

138 hours of drying at 60°C. Polyimide surface modification is illustrated in Fig S1.

2.5. Immobilization of enzyme on polyimide aerogel

140 At room temperature ($20 \pm 3°$ C) under vigorous stirring, surface-modified polyimide aerogels were

141 immersed in a glutaraldehyde solution (25%). Then, distilled water was used to remove the

142 unreacted glutaraldehyde from the aerogels. As a second step, glutaraldehyde-activated polyimide

143 aerogels were dried at 60 °C for ten hours. Polyimide aerogels activated with glutaraldehyde were

144 suspended in citrate-phosphate buffer (pH 6.0) containing a known amount of enzyme in 50 mL

145 flasks. At room temperature, the covalent immobilization process was carried out over a period of

146 12 hours while shaking at 450 rpm. Fig S1 illustrates the process of immobilizing enzymes on

147 polyimide aerogels. In addition to determining the enzyme activity in the supernatant, we measured

148 the activity of the enzyme on immobilized polyimide aerogels.

149 For comparison, target enzymes were immobilized using adsorption. For this purpose, known

150 amounts of enzyme solution were added to the citrate-phosphate buffer (pH 6.0) in which 1 g

151 polyimide aerogels were suspended. For a period of 12 hours, the specimen was immobilized with

152 shaking at 450 rpm at room temperature.

153

2.6. Enzyme assay

155 To obtain the enzyme solution for immobilization in polyimide aerogel, the crude extracts

156 produced from promising consortia included intracellular enzymes (i.e., naphthalene dioxygenase

157 (NDH), catechol 2,3 dioxygenase (C2,3D)) were characterized (Kadri et al., 2018a; Kadri et al.,

158 2018b; Kadri et al., 2018c) by the spectrophotometric method as described in our previous work

159 (Davoodi et al.). In brief, the activity of naphthalene dioxygenase was estimated by determining

160 the formation of indigo at 500 nm per time unit. An enzyme reaction was carried out using 5 μl

161 of indole 100 mM as a substrate in the presence of free enzyme solution or 1 g modified polyimide

162 aerogels after enzyme immobilization on its surface (separate tubes) and the reaction was
163 performed at 15 ºC.

164 After measuring the activity of free and immobilized enzymes, immobilization and protein
165 loading yields were determined for the evaluation of immobilization efficiency using Eqns. (1),
166 and (2) as given below (Miri et al., 2021b):

167 $$Protein\ loading\ yield\ (\%) = \frac{Amount\ of\ protein\ loaded}{Amount\ of\ protein\ introduced} \times 100 \tag{1}$$

168 $$Immobilization\ yield\ (\%) = \frac{Amount\ of\ enzyme\ loaded}{Amount\ of\ enzyme\ introduced} \times 100 \tag{2}$$

169 Using 35 mg of immobilized enzymes in 1 mL of sodium phosphate buffer (pH 7.0), continuous
170 stirring was performed for 48 hours. An enzyme activity test was performed by centrifuging the
171 mixture at 16,000 g at 4°C, followed by the analysis of the supernatant (Davoodi et al.).

2.7. Anthracene degradation by NDH and C2,3D immobilized on polyimide aerogels

174 A batch test was conducted in contaminated water to evaluate the behavior of enzymes loaded on
175 polyimide aerogels as materials to remove PAHs (i.e., anthracene) from aqueous media. In a 50-
176 mL flask, a known amount of immobilized enzyme on polyimide aerogel was dispersed in 20 mL
177 of anthracene solution (20 mg/L) and stirred at 200 rpm for 30 hours since previous tests indicated
178 that after 24 hours, the removal rate was negligible. After decanting the supernatant (10 min and
179 11, 000 ×g), PAHs removal efficiency was determined using the initial and final aqueous phase
180 concentrations. Additionally, 5 mL of methanol was mixed with the samples, and then they were
181 sonicated for ten minutes for 10 minutes and a 250-rpm incubation was carried out at room
182 temperature for 8 hours to desorb PAHs from immobilized enzymes on polyimide aerogels.

183

2.8. Fixed bed column system (FBC)

185 In order to study the degradation rate of anthracene by enzyme-bound aerogel, a continuous FBC
186 was planned and built. Test columns were composed of Teflon tubes with an inside diameter of 51
187 mm and a length of 151 mm. Fig S2 illustrates a schematic diagram of an FBC system. As can be
188 seen in the Figure, there is a small tube located at the center of the spiral baffle that extends the
189 entire length of the column and baffle. In the FBC, PAH-contaminated effluent was pumped at a
190 constant flow rate. As a result of an experimental design based on surface response method (RSM),
191 we investigated the impact of initial anthracene concentration, aerogel size and flow rate during
192 the continuous degradation process.

2.9. Removal capacity is the FBC analysis by mathematical equations

194 The anthracene removal efficiency of the enzyme-loaded aerogel and capacity of aerogels were
195 studied by measuring both the influent (C_0) and effluent concentrations of the target pollutant as a
196 function of time, breakthrough point ($\frac{C_{t,out}}{C_o} = 0.5$) and saturated point $\left(\frac{C_{t,out}}{C_o} = 0.95\right)$. The
197 breakthrough time is calculated by numerically integrating the area above the breakthrough curve
198 Eq. (3)

199 $$m_{removal} = \frac{Q_f C_o}{m_B} \int_{t=0}^{t=t_{total}} \left(1 - \frac{C_{t,out}}{C_o}\right) dt \tag{3}$$

200 Where m_B represents mass adsorbent. During each experimental run, the breakthrough curve is
201 derived from the concentration versus time data collected during the experiment. An investigation
202 of the performance of a fixed bed treatment column was conducted using a breakthrough curve.
203 This curve is a plot of the duration of the test against the anthracene concentration in the effluent
204 stream of an target contaminant and water mixture (Davoodi et al., 2021).

205

206 **2.10.   Experimental design**

207 The Response Surface Methodology (RSM) was used to optimize experimental conditions and
208 reduce the number of experiments. We conducted experiments based on the Box-Behnken (BBD)
209 method with three independent variables, coded at three levels between − 1, 0, and + 1. In
210 comparison to other experimental designs, BBD is often considered to be more efficient. BBD
211 method is one of these methods, which is a quadratic design based on incomplete three-level
212 designs. Using this method, it is possible to estimate the value of the features in a quadratic model,
213 designing the necessary experiments, and providing the values of the characters. Based upon the
214 repetition of the center point and the hypothetical points at the midpoint of each side of the cube,
215 this design might be described as a cube design with points at the midpoint of each side. As a result
216 of this design, it is possible to model the response by fitting a second-order polynomial, which can
217 be expressed as follows:

$$Y = \beta_0 + \sum \beta_i X_i + \sum \beta_{ii} X_i^2 + \sum \beta_{ij} X_i X_j \tag{4}$$

218 This model consists of a constant and a linear coefficient, a binary interaction coefficient, and an
219 interaction coefficient between the input variables Xi and Xj (Zhong and Wang, 2010). Based on
220 Eq.5, the above equation can be expressed as a matrix:

$$Y=bX+\varepsilon \tag{5}$$

221 It is calculated by formulating the parameter Y as a vector of the measured values, along with the
222 parameters X as a vector of independent variables. Matrix b is the coefficient matrix, and the
223 parameter X represents the vector of the errors in the experiment. Using the matrix method, Eq.6
224 can be solved as follows:

$$b = (X'X)^{-1} X'Y \tag{6}$$

225 X' represents the transposition of X, and $(X'X)^{-1}$ represents the inverse of the matrix (X'X) (Aslan
226 and Cebeci, 2007). As a result of the Box-Behnken method, Eq. 7 is used to determine the number
227 of experiments.

$$N = w^2 + w + n \tag{7}$$

228 W represents the number of test factors, and n represents the number of iterations around the center
229 point. Coded values are related to real values in the following manner:

$$x_i = \frac{X_i - X_0}{\Delta X_i} \tag{8}$$

230 In the example, χ_i and X_i are the encoded and real independent values, X_0 is the real value of the
231 independent variable at the center point, and ΔXi is the step change of Xi (Amenaghawon et al.,

232 2013). In order to estimate pure error, the experiment was conducted with three central points in
233 15 runs. As shown in Table 1, the BBD was employed to determine the relationship between the
234 obtained results of removal efficiency and operational variables including inlet concentration (X_1),
235 aerogel size (X_2), and flow rate (X_3).

236 Following the development of the model, a sensitivity analysis should be conducted to determine
237 how different values of these parameters affect the output. As illustrated in the following
238 equations, the sensitivity of removal efficiency can be determined by considering the change in
239 the value of operating parameters including aerogel size, flow rate and initial concentration from
240 $\pm 2\%$ to $\pm 30\%$.

241

242 $$Sen_1(\%) = \left| \frac{Removal\ efficiency\ (Aerogel\ size \pm 30\%, F, C_O) - Removal\ efficiency\ (Aerogel\ size, F, C_O)}{Removal\ efficiency\ (Aerogel\ size, F, C_O)} \right|$$

243 (9)

244

2.11. Characterization of aerogels

246 For the analysis of chemical interactions in polyimide aerogels following surface modification and
247 enzyme immobilization, FT-IR spectra were recorded with a Nicolet IS50 FT-IR Spectrometer
248 from Thermo Scientific (USA) (Simón-Herrero et al., 2019).

2.12. Analytical methods

250 The tricyclic aromatic hydrocarbon anthracene was found in high concentrations in the upper water
251 column under floating oil following the spill (Forth et al., 2021). In order to determine the factors
252 that affect the biodegradation potential of PAHs in the environment, anthracene is used as a
253 prototypical PAH (Moody et al., 2001). GC-MS analyses (Agilent model 6890 GC, 5973 MSD)
254 were conducted on specific days following the crude oil spill to confirm the release of anthracene
255 into the water as well as the biodegradation of anthracene in the presence of pre-selected strains
256 and enzyme solutions as described elsewhere (Li et al., 2021).

2.13. Statistical analyses

258 To evaluate the effect of independent variables on response performance (anthracene removal
259 efficiency), and to predict the optimal response value, Design Expert® software Trial
260 Version11.0.3.0 (Stat-Ease Inc., Minneapolis, MN, USA) was employed as an RSM based on the
261 Box-Behnken design (Miri et al., 2022).

262

263

3. Result and Discussion

3.1. Characterization of polymeric support material

Fig 1 illustrates the FT-IR spectra of PAA, polyimide, aminated polyimide, glutaraldehyde-attached polyimide, and enzyme-immobilized polyimide.
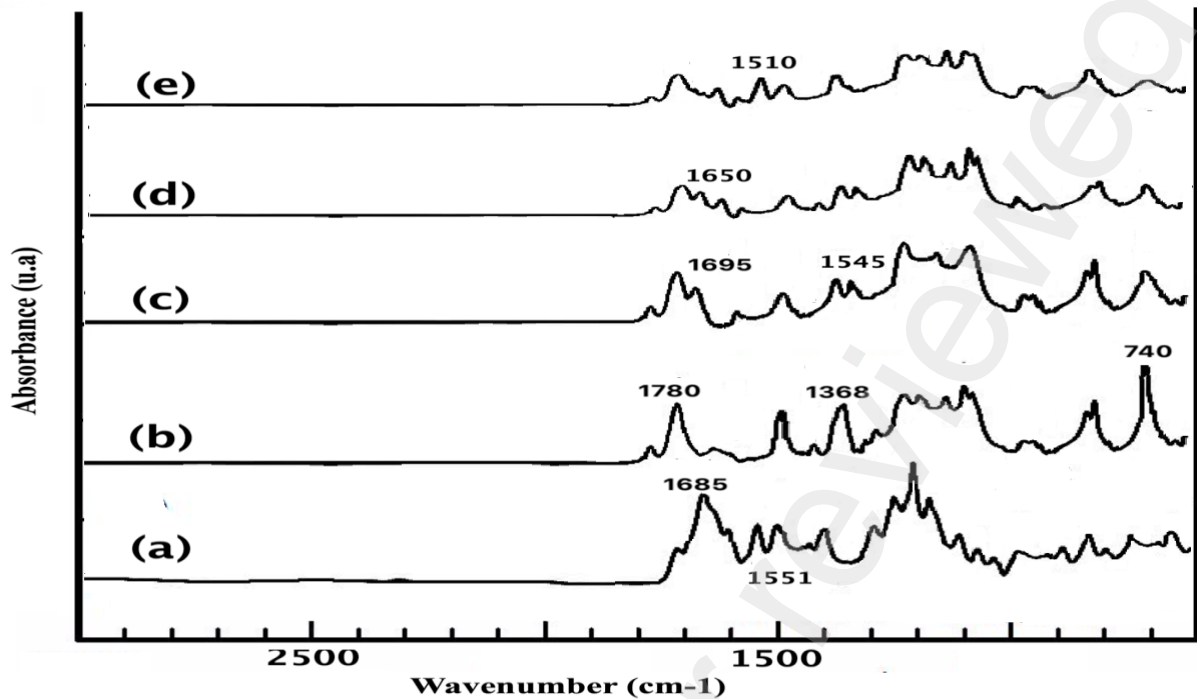
Figure 1 FTIR spectra of a) PAA b) Polyimide aerogel; c) Aminated polyimide aerogel; d) Aminated polyimide aerogel activated with glutaraldehyde and e) Enzyme Immobilized on polyimide aerogel.

At 1685 cm^{-1}, PAA displays the characteristic NHCO peak. A characteristic imide absorption band has been observed in polyimides after imidization at 740 cm^{-1}, 1368 cm^{-1} and 1780 cm^{-1} representing imide IV (bending vibration of cyclic C=O), imide II (C-N stretching vibration), and stretching vibration of cyclic C=O (imide I), respectively (Fig.1. (b)) (Kim et al., 2013). The amination reaction between ethylenediamine and the polymeric support material, and the subsequent creation of amino groups resulted in the formation of new peaks at 1690 cm^{-1} as can be seen in Fig 1. (c). During the formation of polyimide, reaction between amine nucleophilic agent and electrophilic imide group, leading to the opening of the imide ring and the formation of an amide (Çakmakçı et al., 2014). As a next step, glutaraldehyde was used to activate amino groups on the surface of polyimide to facilitate enzyme bonding. This spectrum indicates amide bonds formation because of imide rings cleavage on polyimide surface and the reaction between HMDA's amine groups with the carboxyl group of the imide ring at 1650 cm^{-1} (cracking) and 1546 cm^{-1} (bending) (Çakmakçı et al., 2014). An imide peak is observed in the spectrum of aminated polyimide aerogels activated with glutaraldehyde. This peak was attributed to the interaction between amino groups and glutaraldehyde . In addition to the carbonyl band disappearing after immersion in glutaraldehyde, a new peak was observed at 1659 cm^{-1} after the sample was exposed to glutaraldehyde. As a result of the reaction between glutaraldehyde and free amine groups, It was believed that this band was caused by newly formed imine groups (Schiff-base).

The amide I and II bands of enzymes immobilized on polyimide aerogel were observed at 1510 cm^{-1}. The amide I at 1650 cm^{-1} was primarily attributed to stretching vibrations C=O and the amide II at 1510 cm^{-1} was attributed to stretching vibration CN and bending vibration NH in

293 loaded enzymes. Consequently, amination, activation, and immobilization have been successfully
294 accomplished (Simón-Herrero et al., 2019).

295 **3.2. Enzyme immobilization on polyimide aerogel**

296 As mentioned previously, the strains used for enzyme production are newly isolated *Pseudomonas*
297 URS-5, URS-6, URS-8 and *Rhodocucus* URS-10 as described in detail in our previous work
298 (Davoodi et al.) . The cell extracts obtained from co-culture contains 4 different types types of
299 enzymes involved in PAHs degradation including dioxygenase, hydroxylase, aldehyde
300 dehydrogenase, decarboxylase (Miri et al., 2022). In this study, the performance of immobilization
301 of two key enzymes including naphthalene and catechol 2,3 dioxygenase were studies. Cell extract
302 from newly isolated strains showed high activity of naphthalene and catechol 2,3 dioxygenase.
303 Naphthalene dioxygenase is the key enzyme involved in the initial attack (upper pathway) on
304 anthracene after which anthracene is converted to metabolites (ring oxidation products). Catechol
305 dioxygenase is able to open the ring with an oxidative cleavage and produce ring cleavage products
306 (lower pathway) (Parales et al., 2000).

307 A variety of immobilization methods were used to immobilize PAH degrading enzymes onto
308 polyimide aerogels. Table S1 shows loading of total protein, specific activity and their yield for
309 adsorption and covalent methods. Results suggest that the bound enzymes were active after the
310 immobilization. As can be seen in Table S1, covalent immobilization gave the highest
311 immobilization yield for total protein. Also, it was observed that for adsorption immobilization,
312 less than %23 of the total protein was immobilized. The leaching of enzymes from covalently
313 immobilized enzymes was less than %13 for both target enzymes after 1 h of incubation in turn
314 results in immobilized enzyme stability and subsequent reusability in aquatic media. Thus,
315 comparing the leached enzyme immobilized in modified and unmodified polyimide aerogels
316 showed that covalent bonding prevents leaching and improves enzyme stability (Simón-Herrero
317 et al., 2019; Miri et al., 2021b).

318

3.3.   Storage stability

320   Residual activities of free and immobilized enzymes were determined for up to 16 days at 20 °C.

321   An important aspect of ensuring a long shelf life of an enzyme is its ability to maintain its stability

322   during storage. Enzymes in their free form are generally unstable during storage, and their activity

323   gradually decreases (Miri et al., 2021a; Miri et al., 2021b; Miri et al., 2022). Fig 2 presents the

324   results. The results indicated that the immobilized enzymes on polyimide aerogels demonstrated

325   better storage stability than corresponding free enzymes after 16 days of storage. Naphthalene and

326   catechol 2,3 dioxygenase activity were reduced by 19% and 27% for immobilized enzymes and

327   60% and 73% for free enzymes during the first storage period (6 days). In addition, free

328   naphthalene, and catechol 2,3 dioxygenase have shown a 96% and 81 %reduction in activity after

329   16 days of storage, while immobilized enzymes shows a 58% and 39% reduction in activity after

330   16 days.

331

332
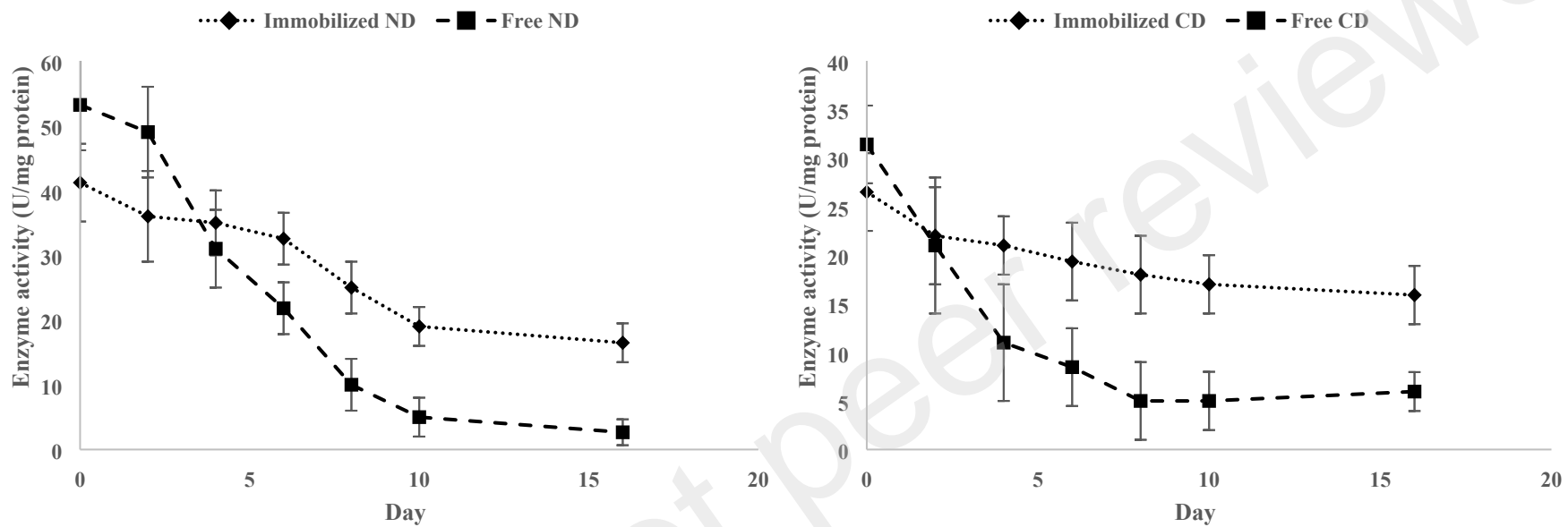
333
334

335   **Figure 2** Effect of time on activity of free and immobilized: (a) naphthalene dioxygenase and, (b) catechol dioxygenase.

336

337

3.4.   Effect of operating parameters on breakpoint time

339

3.4.3. Effect of inlet concentration

The influence of influent PAH concentration (10, 30, 50 mg L^{-1}) upon the degradation efficiency of the fixed bed column containing the aerogel specimens was examined. As illustrated in Fig 3a, an increase in the inlet anthracene concentration from 10 to 30 mg L^{-1}, which can influent contact time, results in the increase in removal capacity of the column from 4.9 to 27.3 mg g^{-1}. In this case, the probability of contaminant contacting enzymes increased with an increase in initial anthracene concentrations, and the driving force and the rate at which anthracene passed across the boundary layer from the bulk solution to the particle surface. However, to avoid many contaminants in the outlet at high concentrations of anthracene that resulted in a lot of unused capacity, 30 mg L^{-1} was considered as desired concentration (Lonappan et al., 2019; Davoodi et al., 2021).

351

3.4.2. Effect of flow rate

The contact time between the surface of enzyme loaded aerogels and the solute is determined by this parameter; thus, it plays an important role in the design of a fixed bed column. Fig 3 illustrates the effect of flow rate on the breakthrough curve following the arrival of contamination and retardation of anthracene following the plug flow pulse (Davoodi et al., 2021). Two phenomena usually occur as the flow rate decreases: 1) the flow was travelling less quickly, so it would be delayed, and 2) the column becomes saturated after breakpoint time (Davoodi et al., 2021). Based on our results, the breakpoint time decreased from 432 to 245 min as the feed flow rate increased from 15 to 25 mL/min, while the removal capacity decreased from 27 to 21 mg/g (22% decrease).

3.4.1. Effect of aerogel size

For columns with a constant flow rate of 15 ml min^{-1} and initial anthracene concentration of 10 mg l^{-1}, Fig 3 illustrates the effect of enzyme-loaded aerogel size on the distribution of anthracene concentration at effluent and arrival time. The cubic aerogels are considered 2, 3 or 4 cm in length. Changing the particle size might have a significant impact on the amount of surface area that can be achieved and number of loaded enzymes. Our results showed that as the size of cubic aerogels decreased the breakpoint time increased from to min and the breakthrough curve steepness increased which is favorable for fixed bed columns. the probability of contaminant contacting enzymes increased with an increase in initial anthracene concentrations.

370

371

372

373

374
375

376
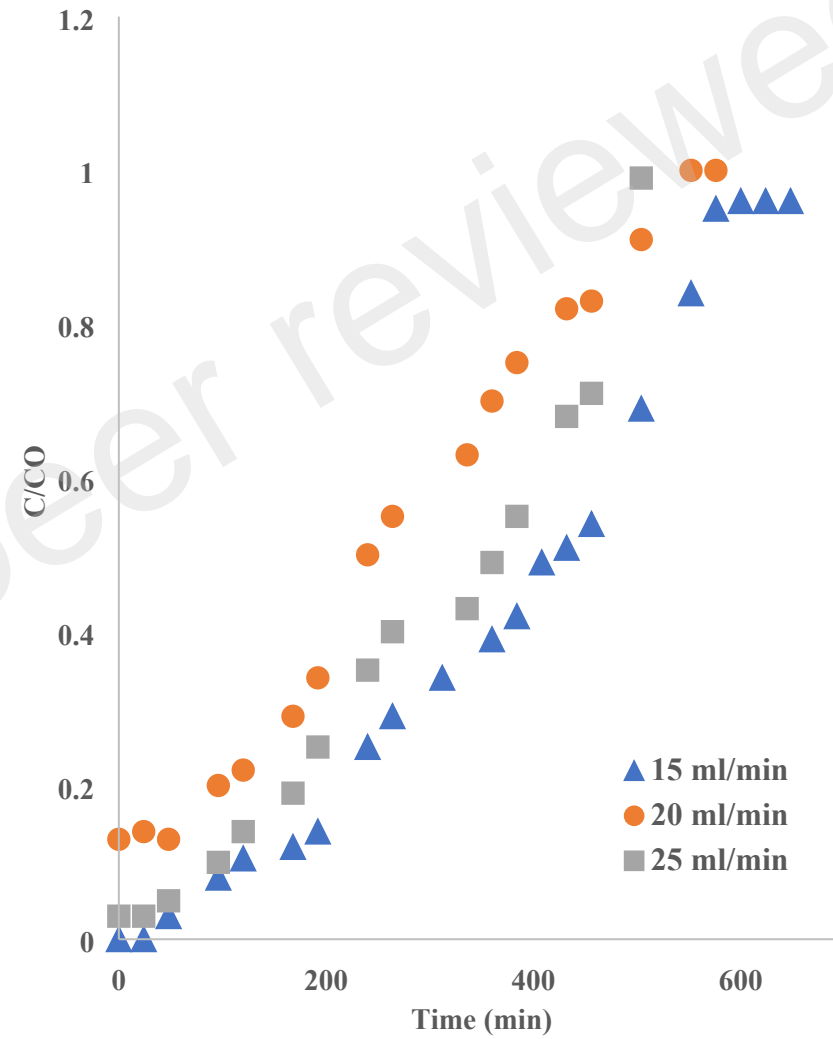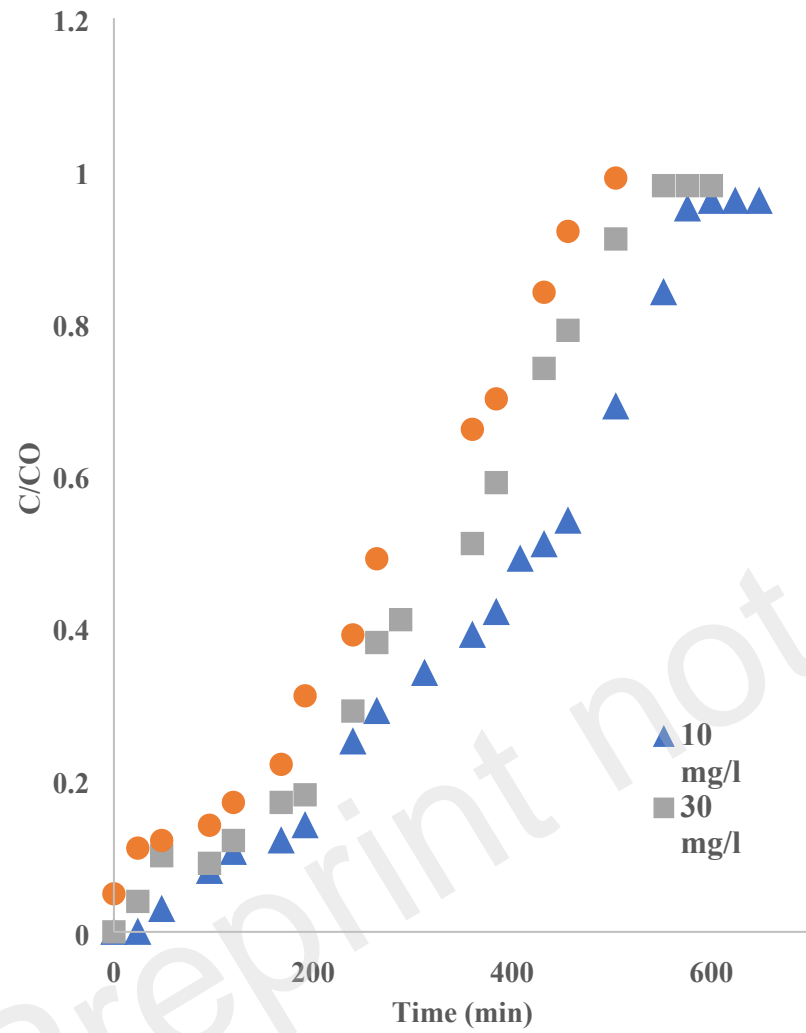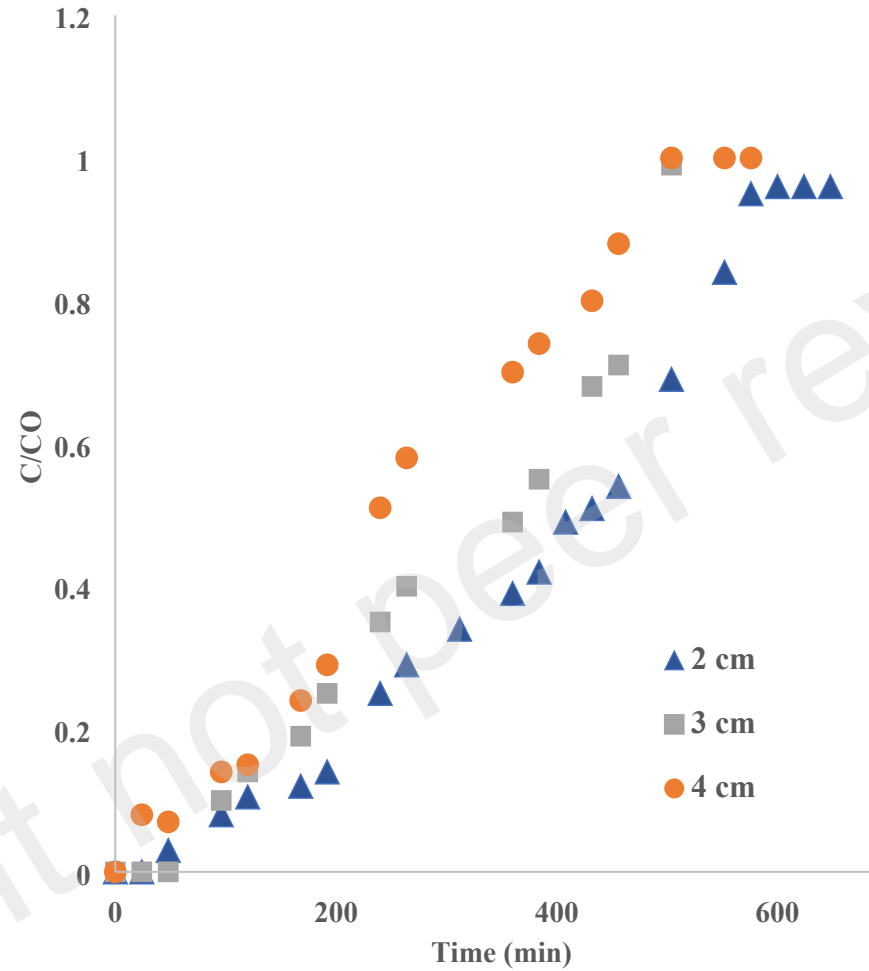
Figure 3 Effect of: (a) initial inlet anthracene concentration (aerogel size 2 cm and flow rate 15 ml min^{-1}); (b) flow rate (aerogel size 2 cm and influent concentration 10 mg l^{-1}); (c)

aerogel size (influent concentration 10 mg l^{-1} and flow rate 15 ml min^{-1}) on the breakthrough curve for anthracene removal using enzyme-loaded aerogel

379

3.5. Design of Experiment

Table S2 presents the actual and coded values of 15 experimental runs related to the Box-Behnken design method. Using a quadratic polynomial model, the mathematical relationship between the response (ion removal efficiency %) and three independent variables (inlet anthracene concentration, size and flow rate) was simulated. Eq.7 was derived from the model based on the second-order polynomial equation (Eq. (10)).

$$Removal\ efficiency\ (\%) = 269.1\ x_1 - 0.75\ x_2 - 2.5\ x_3 + 0.01\ x_1 x_2 + 0.2\ x_1 x_3 + 0.12 x_2 x_3$$
$$- 21.1 x_1^2 - 505.15 \qquad (10)$$

Using the analysis of variance (ANOVA) and R^2, the gained quadratic equation was determined by the best fitting of experimental data (Mourabet et al., 2012). ANOVA analysis is a prominent step in the BBD method which is presented in Table 1.

Table 1. ANOVA results obtained from design of experiment

Source	Sum of Squares	Mean Square	F-value	p-value
Model*	3873.2	399.3	288.13	< 0.0001
X_1- Initial Concentration (mg L^{-1})	299.1	306.1	110.49	0.0002
X_2-Aerogel size	329.3	331.9	102.70	0.0002
X_3-Flow rate	150.1	125.4	242.04	< 0.0001
$X_1 \times X_2$	6.1	6.9	3.55	0.0316
$X_1 \times X_3$	8.4	5.6	6.19	0.0453
$X_2 \times X_3$	6.9	8.3	5.66	0.1043
X_1^2	0.0201	0.0191	0.0103	< 0.0001
X_2^2	2704.1	2937.2	1453.3	0.6943
X_3^2	0.2840	0.2732	0.2402	0.4091
Residual	8.33	1.77		
Lack of Fit**	4.89	1.80	2.55	0.5114
Pure Error	1.48	0.9103		
Correlation Total	3810.29			

* significant   ** not significant

There is a reasonable connection between the response and the parameters, as indicated by the F and P-values, and the parameter and response data agree. There was a greater than 0.001 F-value for the model (288), indicating that the model is significant. Since flow rate has an F-value of 242, which is higher than the F-value of the two other variables, flow. rate is more effective in influencing the output response. Significant model terms are those with a P-value less than 0.05 ; however, when it is greater than 0.1, the model is insignificant. The table indicates that the variables (initial concentration, aerogel size, flow rate, initial concentration *aerogel size, initial

402 concentration*flow rate, aerogel size* flow rate) were significant with very small P-
403 values(p=0.05). Considering the P-value of 0.51, there appears to be a lack of fit in the model,
404 which indicates that the difference between the pure error and the P-value is not significant. In the
405 correlation total and residual values, the sum of each column is represented by the correlation total
406 and the difference between the experimental and predicted data is represented by the residual value
407 (Chen and Wang, 2004).

408 Using the models, the anthracene removal efficiency was predicted within the experimental range
409 with an R^2 value of 0.989, which was in good agreement with the predicted R^2. Based on the
410 adjusted R^2 value of 0.978, only 0.43% of the variation is not explained by input variables (Ma et
411 al., 2018). For a reasonable agreement, the adjusted and predicted R^2 should be within
412 approximately 0.20 of each other. Otherwise, it is possible that either the data or the model is
413 flawed. There is a reasonable agreement between the predicted and adjusted R^2 (Mei et al.,
414 2016). As an indicator of the degree of precision, the coefficient of variation (%) was 3.98%. An
415 experiment with a relatively low coefficient of variation indicates that the experiment was highly
416 reliable. As indicated by the reported standard deviation (1.09), the values are close to average,
417 that is, their dispersion is low. According to this study, the derived model's adequacy precision is
418 55.19, indicating it is suitable for application within the design space (Song et al., 2018).
419 Fig 4 compares the actual and anticipated data. As can be seen, for the initial concentration of 30
420 mg l^{-1}, there is a low deviation from experimental values, usually less than 5 and 2.5 %
421
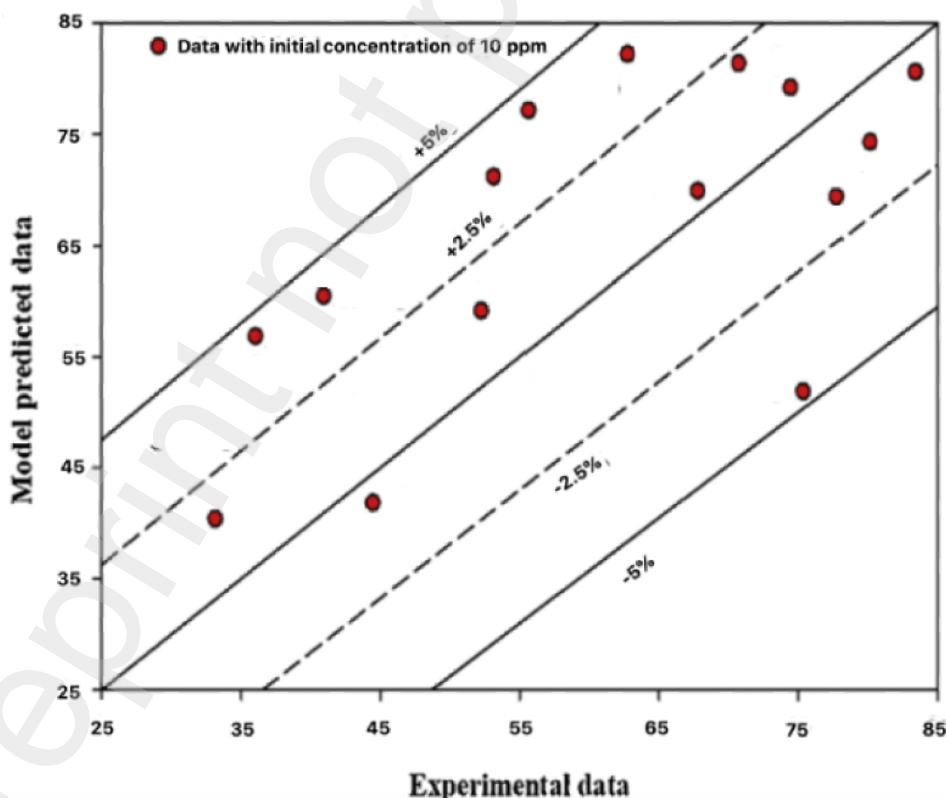
423 **Figure 4** Deviation between calculated and experimental data
424

425 **3.6.   Effect of operating parameters on the anthracene removal**
426

427 Three-dimensional diagrams (Fig 5) illustrate the combined impacts of operating variables on
428 anthracene removal efficiency. Fig 5a and 4b showed the variation of removal efficiency upon

429   variation of flow rate from 15 to 25 ml min^{-1}. The removal efficiency decreased with increasing

430   inlet flow rate from 22 to 30 ml min^{-1}. Additionally, the highest removal efficiency is obtained at

431   a flow rate of 22 mL min^{-1}. Based on Figures 7b and 7c, the removal efficiency decreased as the

432   inlet concentration of anthracene increased, with a maximum removal efficiency at an initial

433   concentration of 34 mg l^{-1}.

434

435
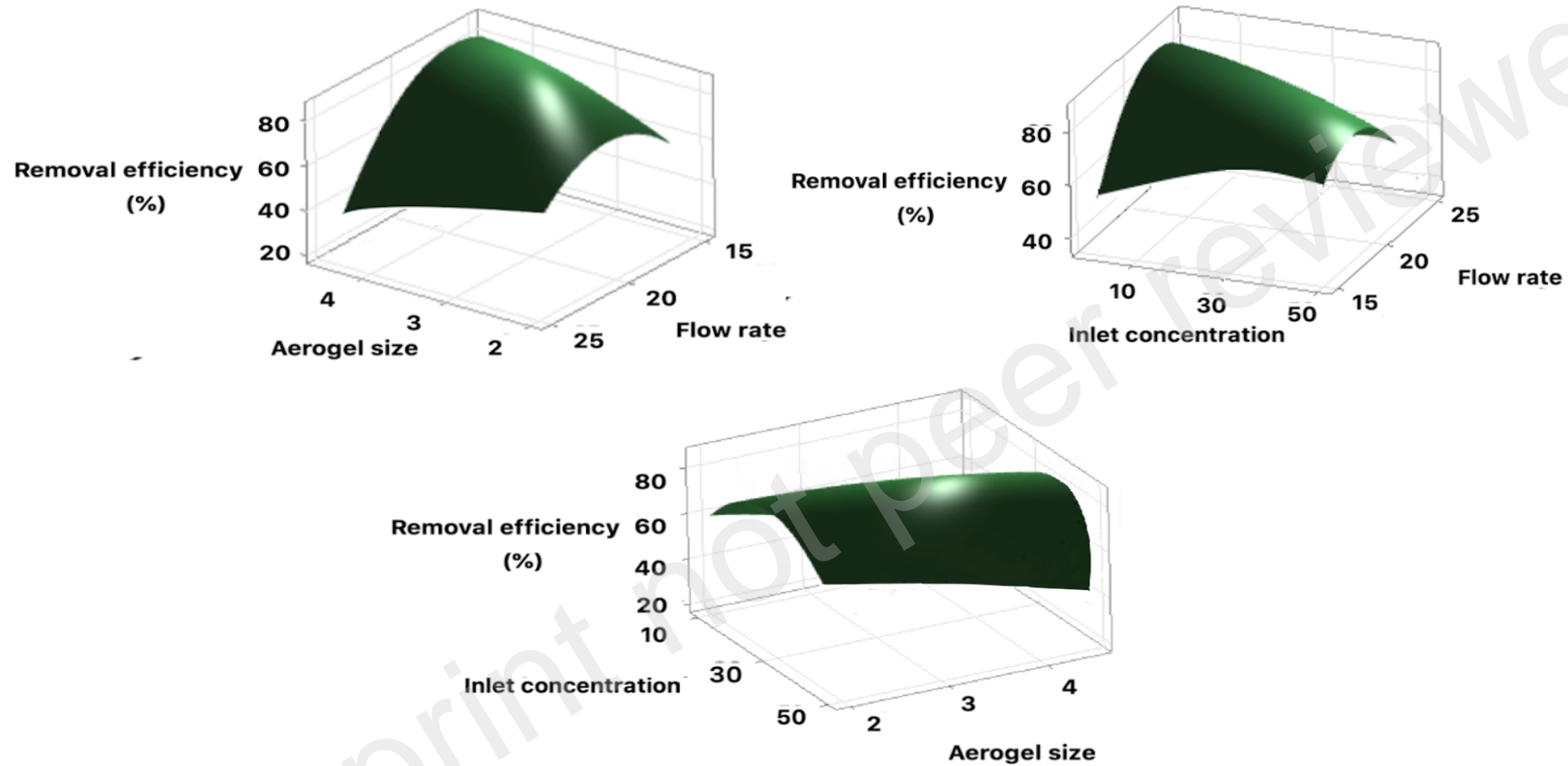
436

437 **Figure 5** Removal efficiency of anthracene based on the: (a) Aerogel size and flow rate, inlet concentration= 10 mg l^{-1} **(b)** Inlet concentration and flow rate, aerogel size = 2 cm **(c)** Inlet

438 concentration and aerogel size, flow rate= 15 ml min^{-1}

A sensitivity analysis was performed on the correlation obtained for removal efficiency (%) to determine the effect of parameters (size of aerogel, inlet concentration, and flow rate). As can be seen in Fig 6, by decreasing the value of flow rate toward 25 ml min^{-1} and decreasing the contact time, considerable changes in the value of removal efficiency can be observed. As mentioned previously, removal efficiency is more sensitive to the flow rate in comparison to aerogel size and inlet concentration of anthracene and as flow rate increases removal efficiency changes more significantly.
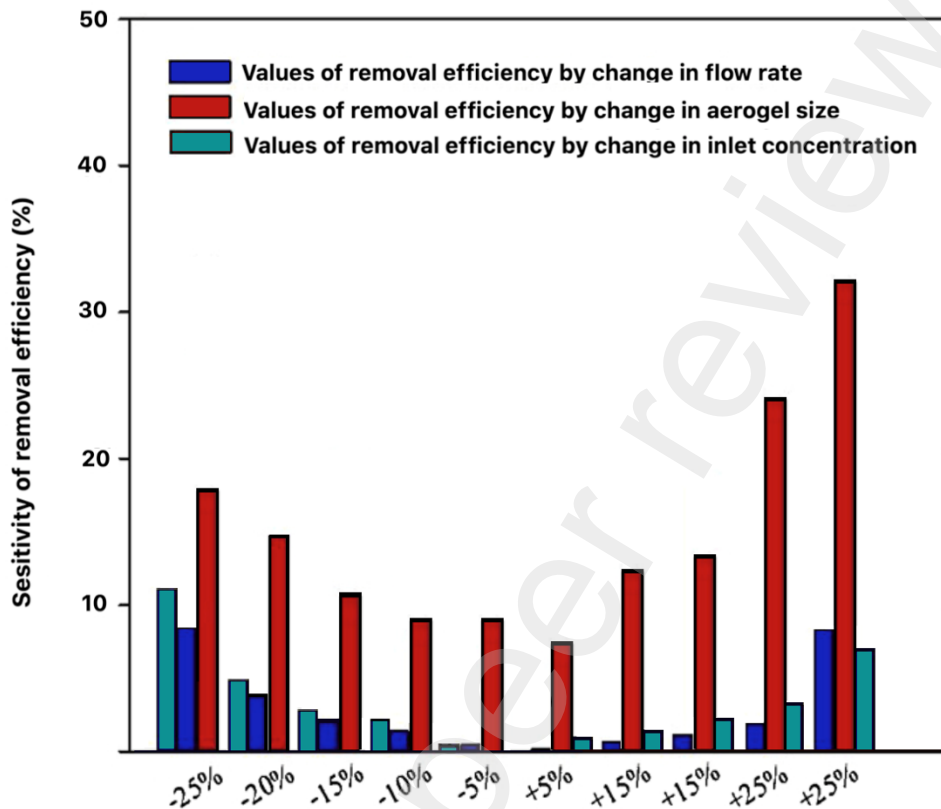
Figure 6 Change in removal efficiency

4. Conclusion

In this paper, we present an experimental study that examines the continuous removal of polycyclic aromatics from water bodies in a fixed-bed column system using an aerogel made of polyimide. Firstly, an investigation was conducted on the covalent immobilization of PAH degrading enzymes on modified polyimide aerogels. Furthermore, the application of prepared immobilized enzymes in fixed bed columns was investigated and the effect of aerogel size, pollutant concentration and flowrate parameters on the removal of target pollutants was examined to determine the optimum parameter values for efficient removal of pollutants using fixed bed columns using the BBD model. Finally, sensitivity analysis was performed on the correlation obtained for removal efficiency (%) to determine the effect of parameters (size of aerogel, inlet concentration, and flow rate). Our results showed that flow rate is more effective in influencing the output response. Moreover, according to the predictions of the derived model, the highest removal efficiency was achieved at a flow rate of 22 ml min^{-1}, an initial concentration of 34 mg l^{-1}, and an aerogel size of 2 cm, however, the removal efficiency was experimentally measured at 87.14 % under these conditions.

478

479 References:

480 Amenaghawon, N., Nwaru, K., Aisien, F., Ogbeide, S., Okieimen, C., 2013. Application of Box-
481 Behnken design for the optimization of citric acid production from corn starch using Aspergillus
482 niger. British Biotechnology Journal 3, 236.

483 Aslan, N., Cebeci, Y., 2007. Application of Box–Behnken design and response surface
484 methodology for modeling of some Turkish coals. Fuel 86, 90-97.

485 Çakmakçı, E., Çiğil, A.B., Danış, Ö., Demir, S., Kahraman, M.V., 2014. Immobilization of
486 alpha-amylase on aminated polyimide membrane: Preparation, characterization, and properties.
487 Starch-Stärke 66, 274-280.

488 Chen, J.P., Wang, L., 2004. Characterization of metal adsorption kinetic properties in batch and
489 fixed-bed reactors. Chemosphere 54, 397-404.

490 Davoodi, S.M., Brar, S.K., Galvez-Cloutier, R., Martel, R., 2021. Performance of packed and
491 fluidized bed columns for the removal of unconventional oil using modified dolomite. Fuel 285,
492 119191.

493 Davoodi, S.M., Miri, S., Kaur Brar, S., Knystautas, E., Martel, R., Simulation of Novel Jellyfish
494 Type of Process for Bioremediation Application. Available at SSRN 4140189.

495 Davoodi, S.M., Miri, S., Taheran, M., Brar, S.K., Galvez-Cloutier, R., Martel, R., 2020.
496 Bioremediation of unconventional oil contaminated ecosystems under natural and assisted
497 conditions: a review. Environmental Science & Technology 54, 2054-2067.

498 Kadri, T., Cuprys, A., Rouissi, T., Brar, S.K., Daghrir, R., Lauzon, J.-M., 2018a.
499 Nanoencapsulation and release study of enzymes from Alkanivorax borkumensis in chitosan-
500 tripolyphosphate formulation. Biochemical Engineering Journal 137, 1-10.

501 Kadri, T., Magdouli, S., Rouissi, T., Brar, S.K., 2018b. Ex-situ biodegradation of petroleum
502 hydrocarbons using Alcanivorax borkumensis enzymes. Biochemical Engineering Journal 132,
503 279-287.

504 Kadri, T., Magdouli, S., Rouissi, T., Brar, S.K., Daghrir, R., Lauzon, J.-M., 2018c. Bench-scale
505 production of enzymes from the hydrocarbonoclastic bacteria Alcanivorax borkumensis and
506 biodegradation tests. Journal of biotechnology 283, 105-114.

507 Kim, S., Jang, K.-S., Choi, H.-D., Choi, S.-H., Kwon, S.-J., Kim, I.-D., Lim, J.A., Hong, J.-M.,
508 2013. Porous polyimide membranes prepared by wet phase inversion for use in low dielectric
509 applications. International Journal of Molecular Sciences 14, 8698-8707.

510 Li, Z., Cabana, H., Lecka, J., Brar, S.K., Galvez, R., Bellenger, J.-P., 2021. Efficiencies of selected
511 biotreatments for the remediation of PAH in diluted bitumen contaminated soil microcosms.
512 Biodegradation 32, 563-576.

513 Lonappan, L., Rouissi, T., Liu, Y., Brar, S.K., Surampalli, R., 2019. Removal of diclofenac using
514 microbiochar fixed-bed column bioreactor. Journal of Environmental Chemical Engineering 7,
515 102894.

516 Ma, S., Yang, X., Wang, C., Guo, M., 2018. Effect of ultrasound treatment on antioxidant activity
517 and structure of β-Lactoglobulin using the Box–Behnken design. CyTA-Journal of Food 16, 596-
518 606.

519 Mei, D., He, Y.L., Liu, S., Yan, J., Tu, X., 2016. Optimization of CO2 conversion in a cylindrical
520 dielectric barrier discharge reactor using design of experiments. Plasma Processes and Polymers
521 13, 544-556.

522 Miri, S., Davoodi, S.M., Brar, S.K., Rouissi, T., Sheng, Y., Martel, R., 2021a. Psychrozymes as
523 novel tools to biodegrade p-xylene and potential use for contaminated groundwater in the cold
524 climate. Bioresource Technology 321, 124464.

525 Miri, S., Davoodi, S.M., Robert, T., Brar, S.K., Martel, R., Rouissi, T., 2022. Enzymatic
526 biodegradation of highly p-xylene contaminated soil using cold-active enzymes: A soil column
527 study. Journal of Hazardous Materials 423, 127099.

528 Miri, S., Perez, J.A.E., Brar, S.K., Rouissi, T., Martel, R., 2021b. Sustainable production and co-
529 immobilization of cold-active enzymes from Pseudomonas sp. for BTEX biodegradation.
530 Environmental Pollution 285, 117678.

531 Moody, J.D., Freeman, J.P., Doerge, D.R., Cerniglia, C.E., 2001. Degradation of phenanthrene
532 and anthracene by cell suspensions of Mycobacterium sp. strain PYR-1. Applied and
533 environmental microbiology 67, 1476-1483.

534 Mourabet, M., El Rhilassi, A., El Boujaady, H., Bennani-Ziatni, M., El Hamri, R., Taitai, A., 2012.
535 Removal of fluoride from aqueous solution by adsorption on Apatitic tricalcium phosphate using
536 Box–Behnken design and desirability function. Applied Surface Science 258, 4402-4410.

537 Murphy, C., 2016. Polyimides. Nova Science Publishers, Incorporated.

538 Parales, R.E., Lee, K., Resnick, S.M., Jiang, H., Lessner, D.J., Gibson, D.T., 2000. Substrate
539 specificity of naphthalene dioxygenase: effect of specific amino acids at the active site of the
540 enzyme. Journal of bacteriology 182, 1641-1649.
541 Rodríguez-Delgado, M., Ornelas-Soto, N., 2017. Laccases: A blue enzyme for greener alternative
542 technologies in the detection and treatment of emerging pollutants. Green Technologies and
543 Environmental Sustainability. Springer, pp. 45-65.
544 Simón-Herrero, C., Naghdi, M., Taheran, M., Brar, S.K., Romero, A., Valverde, J.L., Ramirez,
545 A.A., Sánchez-Silva, L., 2019. Immobilized laccase on polyimide aerogels for removal of
546 carbamazepine. Journal of hazardous materials 376, 83-90.
547 Song, D., Pan, K., Zhang, A., Wu, X., Tariq, A., Chen, W., Li, Z., Sun, F., Sun, X., Olatunji, O.A.,
548 2018. Optimization of growth and production parameters of walnut (Juglans regia) saplings with
549 response surface methodology. Scientific reports 8, 1-10.
550 Zabbey, N., Olsson, G., 2017. Conflicts–oil exploration and water. Global challenges 1, 1600015.
551 Zdarta, J., Meyer, A.S., Jesionowski, T., Pinelo, M., 2018a. Developments in support materials for
552 immobilization of oxidoreductases: A comprehensive review. Advances in colloid and interface
553 science 258, 1-20.
554 Zdarta, J., Meyer, A.S., Jesionowski, T., Pinelo, M., 2018b. A general overview of support
555 materials for enzyme immobilization: characteristics, properties, practical utility. Catalysts 8, 92.
556 Zhong, K., Wang, Q., 2010. Optimization of ultrasonic extraction of polysaccharides from dried
557 longan pulp using response surface methodology. Carbohydrate polymers 80, 19-25.
558 Zucca, P., Sanjust, E., 2014. Inorganic materials as supports for covalent enzyme immobilization:
559 methods and mechanisms. Molecules 19, 14139-14194.
560